Noninvasive Arterial Monitor for Quantitative Oxygen-15-Water Blood Flow Studies

A. Dennis Nelson, Floro Miraldi, Raymond F. Muzic, Jr., Greg P. Leisure and William E. Semple

Division of Nuclear Radiology, Department of Radiology, and Department of Psychiatry, University Hospitals of Cleveland, CWRU, School of Medicine, Cleveland, Ohio

A noninvasive monitor has been developed for monitoring arterial radioactivity in quantitative PET studies of blood flow. The significance of this probe is that quantitative blood flow studies can be performed without the use of arterial catheterization. The method employed is based on the flux of photons emanating from the superior lobe of the right lung following an intravenous bolus of $H_2{}^{15}O$. Calibration of the monitor is obtained by measuring the relationship between lung monitor counts and arterial radioactivity after arterial and venous radioactivity levels have equilibrated following inhalation of $C^{15}O$. To determine the accuracy of the lung probe as a measure of arterial radioactivity, 44 brain blood flow determinations were made in 11 volunteers using arterial radioactivity measures based both on the lung probe and continuous sampling from a radial artery. Repeated measures analysis of variance found no differences between invasive and noninvasive estimates of blood flow. These results suggest that the lung monitor enables quantitation of cerebral blood flow yet avoids the trauma of an arterial puncture.

J Nucl Med 1993; 34:1000–1006

Oxygen-15-labeled water is a commonly used cerebral blood flow (CBF) tracer due to its short half-life, ease of production and use and low toxicity. However, there is no generally accepted method for quantification of CBF using $H_2{}^{15}O$ and *noninvasive* monitoring of arterial radioactivity. Although qualitative CBF images or relative values are often sufficient, for many CBF applications, quantitation of either local or global CBF levels is important. These applications include: evaluation of pre- and post-therapy trials, especially drug evaluations, drug therapy, quantitation of oxygen metabolism and evaluation of various disease states. The present study describes a method that we have used successfully for noninvasive monitoring of arterial $H_2{}^{15}O$ radioactivity using a monitor which records lung radioactivity levels. The validity of this method is determined by comparison to continuous sampling of arterial radioactivity from a radial artery.

Received Jun. 29, 1992; revision accepted Dec. 16, 1992.

For correspondence and reprints contact: A. Dennis Nelson, PhD, Director, Image Analysis Center, Division of Nuclear Radiology, University Hospitals of Cleveland, 2074 Abington Rd., Cleveland, Ohio 44106.

METHODS

Subjects

All 11 subjects included in this study were normal volunteers participating in a study to determine the effects of a fluorinated quinolone (*1*) on cerebral blood volume, blood flow and oxygen and glucose metabolism. Normal subjects were selected by the following criteria: age (18–50 yr), males or surgically sterile females, overall good health, nonsmoker, at least 60 kg in weight, no history of neurologic or psychiatric disease, normal magnetic resonance (MR) image of the brain and urine toxicology screen within 14 days of the PET scan to test for illicit drug use. Caffeine restriction began 48 hr before the base line scan and was continued throughout the study.

In each subject, paired CBF measurements were obtained on the first scanning day and a second pair were obtained 3 days later at a similar time of the day. Three patients were controls and received a placebo between scan days and eight patients received four doses of 200 mg of enoxacin at 12-hr intervals. Enoxacin is a fluorinated quinolone anti-infective currently approved for the treatment of urinary tract infections and uncomplicated urethral or cervical gonorrhea and was studied because of questions concerning possible adverse central nervous system effects. Scans were obtained under conditions of low sensory stimulation using dimmed lights and minimal background noise. This study was approved by the Institutional Review Board of University Hospitals of Cleveland and written informed consent was signed by each subject.

PET Image Acquisition

All positron image data was accumulated with a four-ring, seven-plane Scanditronix SP3000 (Pett Corp., St. Louis, MO) whole-body PET camera with 320 BaF crystals per ring (*2*). This camera records coincidence detection of positron annihilation photons in a list mode manner using time-of-flight (TOF) circuitry which results in positron localization in one of thirty-two 2.31-cm TOF bins. TOF resolution has been measured in our camera as 16 cm full-width half-maximum (FWHM). Attenuation correction was uniquely determined for each subject by obtaining a transmission scan with 13 rotating line sources of germanium-68 arranged in a 45 degree sector. Images were reconstructed for operator selected time intervals of 1 sec resolution using a confidence-weighted backprojection technique (*3*). Intrinsic radial resolution is 4.8 mm FWHM and was 12 mm FWHM in this study, primarily due to filters used for image reconstruction. PET raw data was collected in the low resolution axial mode which resulted in slice thickness profiles that were 11 mm (cross slice) to 13 mm (straight slice) FWHM in the imaging field of interest.

Random events were corrected by measuring detected events

at the periphery of the imaging field (23 cm from the center) and assuming that these events were uniformly distributed across the imaging field prior to attenuation correction. This assumption is valid for our TOF system given that the subject's head extends to approximately 10 cm from the center and TOF resolution is 16 cm FWHM or 8 cm in a radial direction. System dead time was determined with a phantom molded in the shape of a head and filled with an initial concentration of ^{11}C, which resulted in a total system coincidence rate of 350,000 detected coincidences/sec. Images were reconstructed at specific time intervals until the average measured radioactivity in regions placed within the head region of PET phantom images decayed in a log-linear manner with the 20.4-min half-time of ^{11}C. Extrapolation of this line to higher total system count rates resulted in measurement of dead time as a function of total system count rate. During bolus $H_2{}^{15}O$ studies, the total number of counts detected during each second was monitored. This measured count rate enabled dead time correction with a temporal resolution of 1 sec.

Two laser cross-hair imaging systems, aligned to the center of the imaging field and parallel to the detector ring respectively, were used to position the subject's head so that imaging slices were parallel to the orbitomeatal line. The center of the second slice was aligned with the orbitomeatal line. The head was immobilized with a heat-pliant face mask ("polyform", Roylan Industries, Menomenee Falls, WI). The mask was 45 × 12 cm with 2.5-cm eye holes at a center-to-center distance of 6 cm and was softened in a 70°C water bath then molded into a tightly fitting mask that extended from the upper forehead to the tip of the nose.

Invasive Arterial Radioactivity Monitor

An invasive arterial positron radioactivity monitor has been developed (*4*) and used in more than 2000 human PET studies. This monitor provides continuous measures of radioactivity levels in 0.1-sec intervals (see Fig. 3B). A constant flow infusion/withdrawal pump withdraws blood from a radial artery at a volume flow rate of 6 ml/min through a catheter connected to 1-mm inner diameter (i.d.) teflon tubing. The typical length of tubing from the radial artery to the monitor is 25 cm which results in a 2-sec delay. Approximately 20 cm of tubing is wrapped in front of the crystal in two and one half loops of tubing. This tubing is monitored by a scintillation system (Rexon Corp., Beachwood, OH) for gamma counting and is interfaced to a multichannel analyzer (Canberra Industries, Meriden, CT) which monitors photons with energy levels in a 20% window about the 511 keV photopeak. The device sensitivity is greater than 500 (cps) (μCi/ml), corresponding to a peak activity of approximately 10,000 cps for a 50-mCi bolus injection in an adult. The system dead time is 1.2 μsec based on a nonparalyzable model. All monitored counts are corrected for dead time which results in less than a 1.5% correction in counts for the peak counting rate. Calibration is independent of hematocrit and positron energy since only the constant energy 511 keV photons produced by positron annihilation are detected.

In order to determine the dispersion of the bolus due to flow in blood vessels, a series of in vitro experiments were performed. In these experiments, radioactivity was monitored with the invasive arterial monitor following a step input of radioactivity in tubes of various lengths, diameters and volume flow rates. In order to emulate physiologic measurement conditions, the arterial monitor was connected to the tubing with a needle, cannula and three-way stopcock in a manner analogous to that used with a radial artery. The lengths of 3.2 and 6.4 mm i.d. tubing to the point of needle insertion were 90, 45, 20 and 14 cm with volume flow rates of 46, 23, 11 and 6 ml/min. The volume flow rates in both the larger external tubing and the 1-mm tubing used for the arterial monitor were obtained with two separate infusion withdrawal pumps. In each experiment, the volume flow rate to the arterial monitor was 6 ml/min which was also the volume flow rate used for the in vivo studies. For each of 37 experiments, the time delay and exponential time constant which provided the best fit to the measured data was determined using a least squares difference optimization technique. The most consistent parameter for predicting the dispersion time constant was the time delay between the initiation of the step response and the arrival of the bolus at the monitor. A plot of time delay versus dispersion time constant for these experiments is shown in Figure 1. A line of best fit to this data was determined with a least squares technique. The equation for the line of best fit is dispersion time constant equals (2.09/time delay) + 0.027.

Based on these empirical results, the lung monitor curve was dispersed and the invasive monitor curve deconvolved using these time constants in order to more accurately predict arterial bolus shape in the brain. A unit area monoexponential dispersion function was created as suggested by Iida (*4*):

$$(1/a) * \exp(-at),$$

where a is the dispersion time constant and t is time. This function was convolved with the lung monitor curve in order to create the dispersed input function. Similarly, this function was deconvolved from the arterial monitor curve by Nelson (*5*), and a constrained iterative algorithm described by Schafer (*6*).

Simulated tissue curves were generated by applying the water blood flow model to monitor outputs. The bolus arrival at either the brain or the monitor is measured as the point where the slope of either the measured tissue or simulated tissue time activity curve in counts/sec^2 is greater than 0.01 times the peak count rate for the longest time interval (*7*). The delay used for calculation of the dispersion time constant is the difference in bolus arrival times between the simulated monitor tissue curve and the measured tissue time activity curve. The invasive monitor time activity curves are deconvolved using calculated dispersion time constants (Fig. 3F).

Noninvasive Arterial Radioactivity Monitor

A noninvasive arterial radioactivity monitor was designed that monitors 511 keV photons which originate in the superior lobe of the right lung. A NaI crystal and PMT were encased in a 4-cm thick cylindrical lead shield with a 6-mm diameter cylindrical hole in the end of the shield to collimate incoming photons (Fig. 2). Less than 0.1% of the incident 511 keV radiation passes through the lead shield without being scattered. The weight of the monitoring system is 28 kg. The NaI crystal, photomultiplier tube and multichannel analyzer are identical to those described for the invasive arterial monitor. Placement of the monitor 4.5″ below the subject results in approximately a 0.85″ field of view (FOV) at the patient's back and 2.5″ at the patient's anterior chest wall.

The relationship between arterial radioactivity and monitor count rate was determined following inhalation of $C^{15}O$. The amount of $C^{15}O$ inspired ranged between 85 and 105 mCi for all subjects. The radioactivity of a venous blood sample was obtained at approximately 2.5 min after inhalation at which time the arterial and venous radioactivity levels are equilibrated. A calibration constant is then easily calculated from the ratio of the monitor count rate-to-measured venous radioactivity and ranged from 84 to 176 (cps)/(μCi/cc). The mean absolute difference in lung monitor calibration constants for two different imaging days in the

same subject is 18.8%. No attempt has been made to determine the sensitivity of lung monitor calibration to changes in patient position on the same scanning day.

After injection of the water bolus and prior to its arrival in the FOV of the noninvasive monitor, a fairly constant background-count level is observed due to detection of scattered radiation (Fig. 3A). The operator defines the end of this interval which is usually 2–5 sec and the mean count level during this time interval is determined. An exponentially decaying background, with maximum amplitude equal to the mean count level and time constant equal to that of ^{15}O is subtracted from all recorded monitor counts.

The initial portion of the curve from the noninvasive monitor has a markedly different shape than the curve from the invasive monitor (Figs. 3A–3B). The height and width of this initial artifact was noted to vary between patients and with probe placement in a given patient. This artifact appears to be the result of scattered radiation occurring in blood vessels that carry the bolus prior to its arrival in the lungs. In order to eliminate this artifact, the beginning of the curve was determined based on a gamma variate fit to the peak of the curve. The peak of the curve was automatically defined as being that portion of the lung monitor curve which was greater than half of the maximum count rate on the upslope and greater than three-fourths of this maximum on the downslope. The starting point for the fit on the upslope could be modified when the operator determined that the artifact extended beyond this point. The form of the gamma variate function is $a(t + dt)^n \exp[-k(t + dt)]$, where t is time and dt, a, n and k are constants which are obtained by a least squares optimization fit between the measured curve and the fit curve. This technique was tested with curves obtained from the invasive monitor which do not have this artifact (Fig. 3D). The initial portion of the fit curve was substituted for the original curve and used in all subsequent analyses (Figs. 3C and 3E). The original curves have been processed with a seven-point median filter so that the fit curve can be observed in Figures 3C and 3D. Each point in the original curve is replaced with the median value of that point and the three points before and after this point.

Since the arterial radioactivity is dispersed as it progresses from the lungs to the brain, the gamma fit curve was dispersed based on the time delay between the bolus arrival in the lungs and the bolus arrival in the head (Fig. 3E). The delay was calculated as

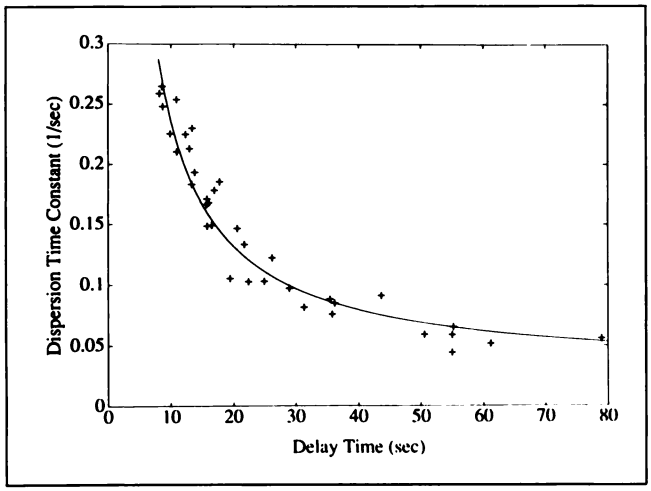

FIGURE 1. Time constant that determines bolus dispersion based on the time that the bolus travels in tubing.

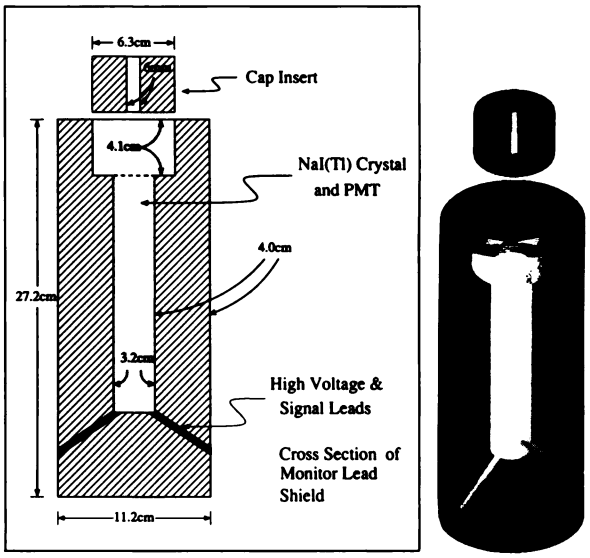

FIGURE 2. Schematic drawing of the noninvasive monitor.

described above for the invasive arterial monitor. Using the same method to calculate takeoff times for both the lung monitor and arterial monitor is valid as the curves have nearly the same shape. A comparison between processed noninvasive and invasive monitor curves is shown in Figure 3G.

Model Description

Brain blood flow was calculated based on an autoradiographic model described by Raichle (*8*) and implemented with a mathematical simplification proposed by Muzic (*9*). The local blood flow is determined by solving:

$$\int_{T_1}^{T_2} C_i(T)\,dT = \lambda k \int_{T_1}^{T_2} \int_0^T C_a(t) \exp[(-k(T-t)]\,dt\,dT, \quad \text{Eq. 1}$$

where Ci(T) is the instantaneous concentration of $H_2{}^{15}O$ in tissue at time T, T_1 and T_2 are the scan start and stop times respectively, Ca(t) is a measure of arterial $H_2{}^{15}O$ concentration at time t, λ is the brain-to-blood equilibrium partition coefficient and $k = (1 - \exp - (PS/f))f/\lambda$, where PS is permeability surface area product and f is blood flow in ml/100 g of tissue/min. The value used for the partition coefficient of water was 0.956 ml/g (*10*). The permeability-surface area product (PS) of water was determined in serial brain blood flow studies with $H_2{}^{15}O$ and ^{15}O-labeled butanol at our institution to be 133 ml/100 g/min (*9*).

A 40-sec image was reconstructed from list mode data with a 1-sec timing resolution using the bolus arrival time in tissue as the start for count integration (*7*). Global brain regions were determined using an objective, automated edge detection technique based on morphological processing. Large blood vessel regions were determined in a $C^{15}O$ scan and removed from global ROIs. The mean global blood flow was defined as the mean flow obtained in global regions for three contiguous brain slices which had the most cortical gray matter. The caudate, putamen, thalamus and frontal cortex were manually identified and regional blood flows generated for both the invasive and the noninvasive monitors.

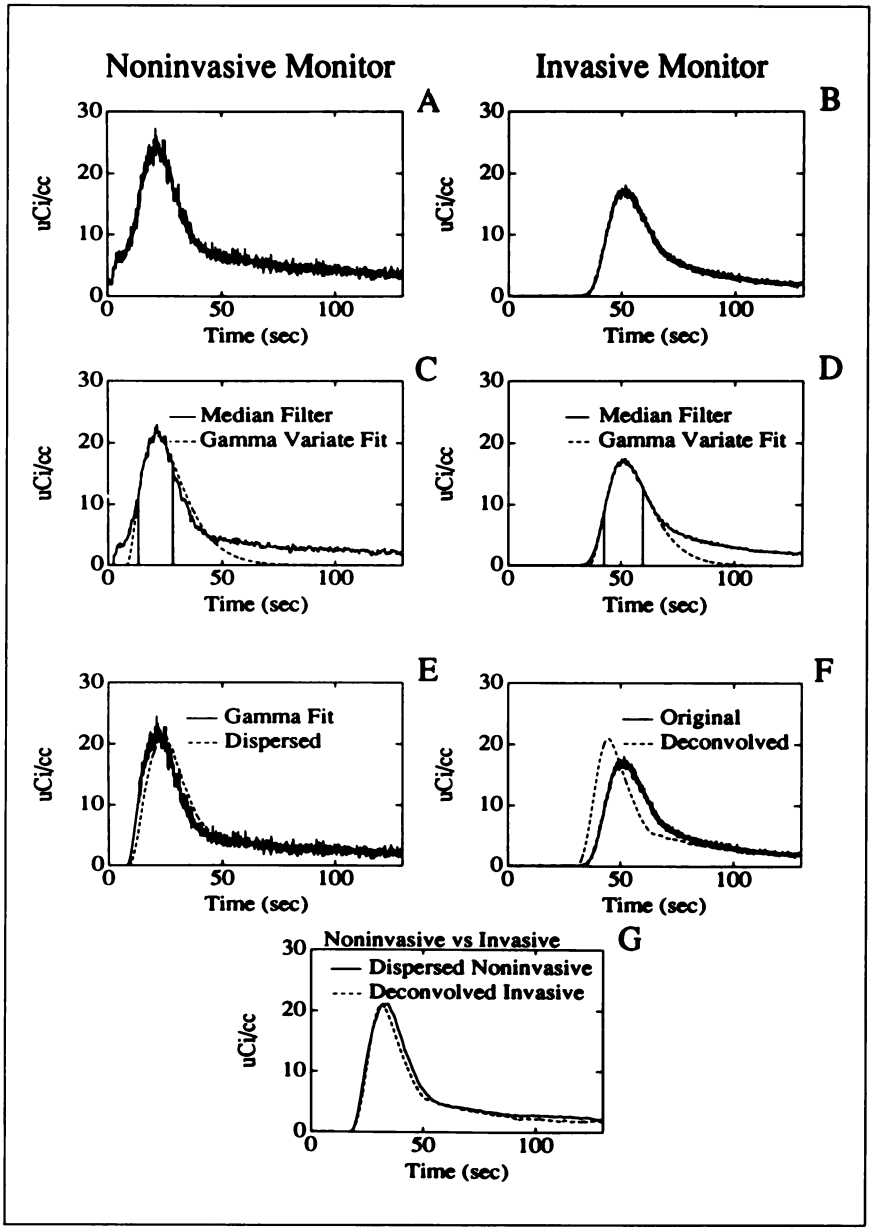

FIGURE 3. Comparison of noninvasive and invasive monitor output. Figures 3A and B depict unprocessed monitor output with 0.1-sec timing resolution. Figure 3D depicts gamma variate fitting with the invasive monitor, whereas Figure 3C demonstrates this fitting with the noninvasive monitor. Figures 3E and F show the effects of bolus dispersion on both the noninvasive and invasive monitor. Figure 3G compares the processed invasive and noninvasive arterial radioactivity curves.

RESULTS

Figure 4 shows the relationship between mean global brain blood flow calculated for both the invasive and noninvasive monitor in 11 volunteers, each with four water blood flow studies. Figure 5 shows the same relationship for regional brain blood flows. The line of identity is displayed in both Figures 4 and 5. Global blood flow measurements for each volunteer are reported in Table 1. The slope and intercept of the simple regression line relating global brain blood flows is 1.015 and 0.841, respectively. Similarly, the slope and intercept for regional brain flows is 0.897 and 6.083. The root mean square error in estimating global blood flows is 3.8 ml/(100 g * min) and this error for regional flows is 3.6 ml/(100 g * min). To determine if the invasive and noninvasive methods differed in the estimation of whole brain blood flow rates, a 2 (invasive versus noninvasive) × 2 (pre-post) × 2 (scan 1–2) repeated measures analysis of variance was performed on the whole brain blood flow rate estimates. There was no effect of invasive versus noninvasive monitoring technique ($F(1, 10) = 0.35$, $p > 0.50$). Mean global flow rate estimates were 54.23 ml/100 cc/min for the noninvasive and 54.73 ml/(100 cc * min) for the invasive monitoring method. There was no effect of pre-post ($F(1, 10) = 0.03$, $p = 0.86$). Mean global flow for the prescans was 54.20 ml/(100 cc * min) and for the postscans was 54.77 ml/(100 cc * min). There was no effect of scan 1–2 ($F(1, 10) = 2.83$, $p = 0.12$). Mean flow for scan 1 was 55.86 ml/(100 cc * min) and for scan 2 was 53.10 ml/(100 cc * min). There were no interactions between any of these main effects.

DISCUSSION

The goal of this study was to develop a noninvasive technique for monitoring arterial radioactivity which can

be applied for quantitation of CBF using $H_2{}^{15}O$. In studies where repeat values are necessary such as pre- and post-therapy and routine clinical studies, use of arterial catheters for arterial radioactivity monitoring is an undesirable feature of PET. Furthermore, brain blood flow responses due both to the sensation and pain associated with the invasive monitor may mask, in certain situations, the blood flow effect of interest. Thus, the development of a noninvasive method has an appeal that makes quantitative PET imaging a more acceptable technique especially in the routine clinical setting. The desire to obtain quantitative blood flow measurements noninvasively has been attempted previously. Celsis (*12*) used a scintillation detector placed over the right lung to obtain the input function to the brain. This study entailed measuring ^{133}Xe using SPECT techniques during and after a 1-min inhalation of ^{133}Xe. The relationship between monitored counts and arterial concentration is obtained by assuming the early ^{133}Xe distribution is proportional to blood flow and scaling this distribution based on the tissue curve obtained from the entire sequence of four 1-min images. Difficulties with quantitation in SPECT images limit the measurement of absolute blood flows in these studies. A PET imaging method has been proposed by Koeppe (*13*) to quantitate CBF without arterial sampling using ^{18}F-labeled fluoromethane which is an inert diffusible gas. This technique uses end expiratory measures of fluoromethane to estimate arterial radioactivity. Disadvantages of the fluoromethane technique include: (1) radiation dose to personnel, (2) required face mask is not easily tolerated by patients and (3) the minimum time between repeat studies is typically 30 min.

The small root mean standard error in our studies between invasive and noninvasive estimates of both whole and regional brain blood flow indicates the equivalence of the noninvasive lung probe and arterial catheter monitoring procedures. Furthermore, inspection of the mean esti-

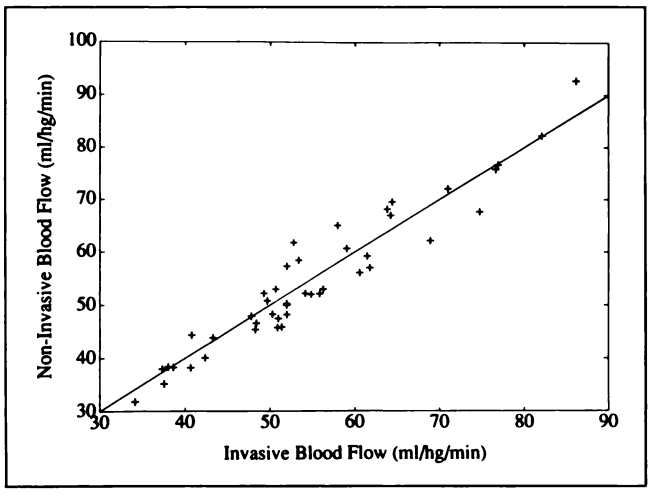

FIGURE 4. Comparison of quantitative global blood flow measurements based on both the invasive and noninvasive arterial radioactivity monitor. The line depicted in the figure is the line of identity.

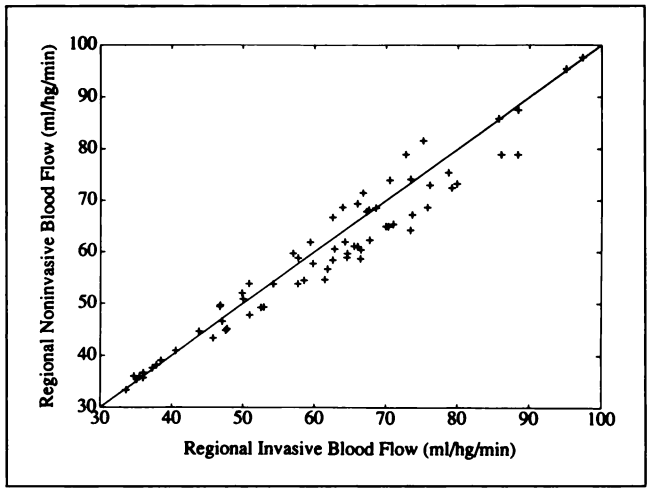

FIGURE 5. Comparison of quantitative regional blood flow measurements based on both the invasive and noninvasive arterial radioactivity monitor. The line depicted in the figure is the line of identity.

mates of global blood flow for the two techniques indicates that differences are very small as well as insignificant.

The method used for dispersion of the lung monitor curve and deconvolution of the arterial monitor curve depend on calculation of dispersion time constants obtained in a series of in vitro experiments. The in vitro experiments do not entirely emulate the physiologic situation since pulsating flow through branching vessels of various diameters and lengths is not simulated. The limitations of this in vitro model do not appear to be significant for brain blood flow calculations based on the similarity of blood flow measurements from both monitors. Iida (*4*) attempted to determine the relationship between time delay and dispersion time constant in vivo by measuring the arterial input function in the left ventricle with the PET camera and simultaneously measuring arterial activity at the peripheral sites of the radial, femoral and dorsal pedis artery. There was a large scatter in the relationship between delay and dispersion with increased dispersion at larger delay times. The in vivo data reported by Iida (*4*) includes the relationship predicted by the described in vitro experiments except at delays less than 7 sec. However, the line of best fit to the data measured by Iida (*4*) predicts less dispersion than that measured by the in vitro study.

An alternative method for calculation of dispersion or deconvolution time constants would be the technique suggested by Meyer (*14*) or Iida (*15*). Both investigators determine three parameters: flow, partition coefficient and time delay. Meyer (*14*) also determines the dispersion time constant which provides the best fit between a measured dynamic tissue curve and a theoretical curve obtained using the above parameters. Use of this technique should improve the relationship of the lung monitor and the arterial monitor curves as both curves would be modified to provide the best fit to the same measured tissue curve. However, use of this technique could also mask real differences between the arterial and lung monitor by account-

TABLE 1
Invasive Versus Noninvasive Water Blood Flow Comparison

Day 1				Day 2			
Study 1		Study 2		Study 1		Study 2	
I	N	I	N	I	N	I	N
47.6	47.6	48.2	46.3	50.7	45.5	54.0	51.9
51.2	45.6	48.1	45.1	61.6	56.7	51.8	50.0
51.8	47.9	42.2	39.8	61.3	58.9	70.9	71.8
37.2	37.7	38.5	38.0	37.4	34.9	34.0	31.5
51.8	49.7	56.1	52.7	58.9	60.4	51.8	57.0
82.0	82.0	64.3	69.3	86.0	92.5	76.5	75.5
76.8	76.4	57.8	64.8	52.6	61.5	54.7	51.7
50.8	47.2	49.5	50.5	40.5	37.9	40.6	44.1
64.1	66.7	63.7	67.9	53.2	58.1	50.1	48.0
60.4	55.8	55.7	51.8	74.6	67.4	68.8	61.9
49.1	51.9	50.5	52.7	37.9	38.1	43.1	43.6

Quantitative global CBF measurements in ml/hg/min for blood flow monitors.
I = invasive and N = noninvasive.

ing for these differences with altered time delays and dispersion time constants. Therefore, this fitting technique was not used for purposes of comparing the monitors in this study.

There are problems with the noninvasive monitor. One problem is background radiation which is currently removed both by using a gamma variate fit for the initial part of the curve and subtracting a monoexponentially decreasing curve with time constant equal to that of ^{15}O. The origin of the background scatter is primarily radiation not in the FOV of the monitor that undergoes one or more scattering events before being detected through the 6-mm aperture. In addition, a small amount of radiation penetrates the lead shield (<0.1% of incident radiation) since the minimum distance through the lead to the crystal is 4 cm. The monoexponentially decreasing correction for scatter is based on the model of a radiation source with uniform geometry and constant location from the monitor. Obviously, this model is not valid for the imaging situation. However, other models that attempt to predict the distribution of radioactivity in the body and their effect on recorded counts are complex and not easily evaluated. The simple proposed solution does seem to work quite well. It is possible to minimize the problem by using both a more highly collimated monitor as well as a smaller energy window to minimize scatter effects. Another potential problem is positioning of the lung monitor. If the probe is positioned too far caudally and centrally, then a cyclic increase and decrease in counts due to breathing and motion of the right atrium in and out of the lung monitor's FOV will be observed. This artifact is easily detected, however, and can be eliminated by moving the probe. Another positioning problem is including large blood vessels which carry blood to and from the heart in the lung probe's FOV. This problem can be easily detected following a small dose of $H_2{}^{15}O$ as an initial spike prior to the main bolus arrival in the lungs.

Currently, calibration of the lung monitor requires an inhalation of $C^{15}O$ which necessitates an additional synthesis, increases the study by 10 min and increases the subject's radiation exposure. For all studies done at our institution, none of these factors is limiting. However, it may be possible to calibrate the lung monitor by taking venous samples approximately 2 min following a water bolus when the arterial and venous radioactivity levels are nearly equal. Finally, there are situations where the monitor may not be appropriate, such as those in which there are interventions that would affect pulmonary blood volume. In such cases, alternative calibration procedures are needed.

In conclusion, a noninvasive method for measuring arterial radioactivity has been shown to be equivalent to the standard technique that employs radial artery catheterization for CBF measurement. This technique may also be applicable for other organs and PET radiopharmaceuticals and may also have application for quantitative SPECT studies.

REFERENCES

1. Bednarczyk EM, Green JA, Nelson AD, et al. Comparative assessment of the effect of lomefloxacin, ciprofloxacin or placebo on cerebral blood flow, glucose and oxygen metabolism in healthy subjects via positron emission tomography. *Pharmacotherapy* 1992;12:369–375.
2. Lewellen TK, Harrison RL, Bice AN. An experimental evaluation of the effect of time-of-flight information in image reconstructions for the Scanditronix/PETT Electronics SP3000 positron emission tomograph—preliminary results. *IEEE Trans Nucl Sci* 1989;36:1095–1099.
3. Politte DG, Hoffman GR, Beecher DE, Ficke DC, Holmes TJ, Ter-Pogossian MM. Image reconstruction of data from super PETT I: a first generation time-of-flight positron emission tomograph. *IEEE Trans Nucl Sci* 1986; 33:428–434.
4. Iida H, Kanno I, Miura S, Murakami M, Takahashi K, Uemura K. A determination of the regional brain/blood partition coefficient of water using dynamic positron emission tomography. *J Cereb Blood Flow Metab* 1989; 9:874–885.
5. Nelson AD, Muzic RF, Muswick GJ, Voelker W, Miraldi F. Continuous arterial positron monitor for quantitation in PET imaging. *Am J Phys Imag* 1990;5:84–88.
6. Schafer RW, Mersereau RM, Richards MA. Constrained iterative restoration algorithms. *Proc IEEE* 1981;69:432–450.

7. Muzic RF, Nelson AD, Miraldi F. Temporal alignment of tissue and arterial data and selection of integration start times for the H_2O^{15} autoradiographic CBF model in PET. *IEEE Trans Med Imag* 1993: in press.
8. Raichle ME, Martin WRW, Herscovitch P, Mintun MA, Markham J. Brain blood flow measured with intravenous $H_2{}^{15}O$. II. Implementation and validation. *J Nucl Med* 1983;24:790–798.
9. Muzic RF, Nelson AD, Miraldi F. Mathematical simplification of a PET blood flow model. *IEEE Trans Med Imag* 1990;9:172–176.
10. Herscovitch P, Raichle ME, Kilbourn MR, Welch MJ. Positron emission tomographic measurement of cerebral blood flow and permeability-surface area product of water using [^{15}O]water and [^{11}C]butanol. *J Cereb Blood Flow Metab* 1987;7:526–542.
11. Berridge MS, Adler LP, Nelson AD, et al. Measurement of human cerebral blood flow with [^{15}O]butanol and positron emission tomography. *J Cereb Blood Flow Metab* 1991;11:707–715.
12. Celsis P, Goldman T, Henriksen L, Lassen NA. A method for calculating regional and cerebral blood flow from emission computed tomography of inert gases concentrations. *J Comp Assist Tomgr* 1981;5:641–645.
13. Koeppe RA, Holden JE, Polcyn RJ, Nickles RJ, Hutchins GD, Weese JL. Quantitation of local cerebral blood flow and partition coefficient without arterial sampling: theory and validation. *J Cereb Blood Flow Metab* 1985; 5:214–223.
14. Meyer E. Simultaneous correction for tracer arrival delay and dispersion in CBF measurements by the $H_2{}^{15}O$ autoradiographic method and dynamic PET. *J Nucl Med* 1989;30:1069–1078.
15. Iida H, Higano S, Tomura N, et al. Evaluation of regional differences of tracer appearance time in cerebral tissues using [^{15}O]water and dynamic positron emission tomography. *J Cereb Blood Flow Metab* 1988;8:285–288.

EDITORIAL

Practical Procedures and Pharmacological Applications of Quantitative PET

As nuclear medicine continues to merge the principles of imaging with those of modern biochemistry, biology and pharmacology, more demanding criteria are placed on measurements being made. The performance of analytical imaging assays of biological processes requires that the methods used have a definable quantitative foundation, whether the end result is a quantitatively reported result in μmole/min/g of tissue or a qualitatively reported clinical evaluation. Although this editorial focuses on the particular issue of ^{15}O-water studies of blood flow with PET, this is an objective for planar gamma and positron cameras, SPECT and PET imaging in nuclear medicine.

There are two levels of quantitation in PET. The first is quantitation of tissue radioactivity concentration as represented by images measured directly by PET scanners. The second is the quantitation of PET images in terms of biological parameters in tissue. The first level involves the consideration of many instrumentation and imaging issues, including scattered radiation, random coincidence, deadtime, photon attenuation, detector efficiency normalization, spatial resolution (intrinsic and reconstructed) and calibration (*1*). The second level requires, in addition, the accurate measurement of time-activity curves (TACs) of labeled compounds in blood/plasma that, combined with the quantitative measurement of radioactivity concentration in tissue and a validated tracer kinetic model, can provide quantitative information on biological parameters of interest in local tissues (*2*).

The measurement procedure of blood TACs is usually invasive, frequently requiring arterial blood sampling that is cumbersome and complex, and deters people from using it on a routine basis. Moreover, it could potentially create unnecessary patient anxiety and thus affect the normal state of the subject being studied. Many approaches have therefore been investigated to make the measurement of blood TACs less invasive and more practical. The paper by Nelson et al. (*3*) is an example of such an approach to minimize the invasiveness of the procedure. The authors used a scintillation probe over the superior aspect of the right lung during a bolus injection ^{15}O-water cerebral blood flow (CBF) study to measure the shape of the ^{15}O-water TAC in arterial blood. The measured TAC was then calibrated to radioactivity concentration units with a calibration study that equated the probe measurement with an equilibrium blood concentration (measured from blood samples with a well counter) following inhalation of ^{15}O-carbon monoxide.

With some clever, but somewhat ad hoc data processings to remove the background and to correct the time shift and dispersion, the probe-measured curve was shown to give estimates of CBF comparable to those obtained using direct arterial blood samples. The use of the probe measurement for ^{15}O-water CBF studies in normals is thus shown to be quite successful.

Some limitations associated with the lung probe approach, however, exist. Some can be easily improved, whereas solutions for others are not so trivial. For example, the use of a separate ^{15}O-carbon monoxide study and blood sampling for calibration is somewhat awkward and the use of ^{15}O with a short half-life of 2 min for calibration is very sensitive to timing errors and background radiation. Although the use of ^{15}O-water for calibration, as suggested by Nelson et al. (*3*), may eliminate the need of the ^{15}O-carbon monoxide inhalation, the high error sensitivity of the calibration due to the short half-life of ^{15}O remains.

The probe measurement for ^{15}O-water CBF studies in normals has been carefully validated by Nelson et al. (*3*). Extension of the approach for studies in patients, with other tracers, or for other organs, however, requires the validation to be repeated for each case, because the applicability of the approach relies on certain special features of the ^{15}O-water tracer that are not common to other tracers/studies.

Received Mar. 5, 1993; revision accepted Mar. 5, 1993.

For correspondence or reprints contact: S.C. Huang, Dept. of Pharmacology, UCLA School of Medicine, Los Angeles, CA 90024-1721.